

C2GM: Cascading Conditional Generation of Multi-scale Maps from Remote Sensing Images Constrained by Geographic Features

Chenxing Sun¹, Yongyang Xu¹, Xuwei Xu, Xixi Fan, Jing Bai, Xiechun Lu¹, and Zhanlong Chen¹

Abstract—Multi-scale maps are essential representations of surveying and cartographic results, serving as fundamental components of geographic services. Current image generation networks can quickly produce map tiles from remote-sensing images. However, generative models designed for natural images often focus on texture features, neglecting the unique characteristics of remote-sensing features and the scale attributes of tile maps. This limitation in generative models impairs the accurate representation of geographic information, and the quality of tile map generation still needs improvement. Diffusion models have demonstrated remarkable success in various image generation tasks, highlighting their potential to address this challenge. This paper presents C2GM, a novel framework for generating multi-scale tile maps through conditional guided diffusion and multi-scale cascade generation. Specifically, we implement a conditional feature fusion encoder to extract object priors from remote sensing images and cascade reference double branch input, ensuring an accurate representation of complex features. Low-level generated tiles act as constraints for high-level map generation, enhancing visual continuity. Moreover, we incorporate map scale modality information using CLIP to simulate the relationship between map scale and cartographic generalization in tile maps. Extensive experimental evaluations demonstrate that C2GM consistently achieves the state-of-the-art (SOTA) performance on all metrics, facilitating the rapid and effective generation of multi-scale large-format maps for emergency response and remote mapping applications. This work has been submitted to the IEEE for possible publication. Copyright may be transferred without notice, after which this version may no longer be accessible.

Index Terms—Generative Cartography, Diffusion Model, Multi-scale Tile Map, Cascading Generation.

This study was supported in part by the National Natural Science Foundation of China under Grant 42471475; the Key Projects of Foundation Improvement Program; the Opening Fund of Key Laboratory of Geological Survey and Evaluation of Ministry of Education (Grant No. GLAB 2024ZR06) and the Fundamental Research Funds for the Central Universities. (*Corresponding author: Zhanlong Chen.*)

Chenxing Sun, and Zhanlong Chen are with the Key Laboratory of Geological Survey and Evaluation of Ministry of Education, China University of Geosciences, Wuhan 430074, China. (e-mail: sunchenxing@cug.edu.cn, chenlz@cug.edu.cn).

Yongyang Xu, Xixi Fan, Jing Bai and Zhanlong Chen are with the School of Computer Science, China University of Geosciences, Wuhan 430074, China.

Zhanlong Chen is with the Engineering Research Center of Natural Resource Information Management and Digital Twin Engineering Software, Ministry of Education, Wuhan 430074, China.

Xuwei Xu is with the School of Geographical and Information Engineering, China University of Geosciences, Wuhan 430074, China.

Xiechun Lu is with the College Of Computer and Information Technology, China Three Gorges University, Yichang 443002, China, and also with the Hubei Key Laboratory of Intelligent Vision Based Monitoring for Hydroelectric Engineering, China Three Gorges University, Yichang 443002, China

Manuscript received April 19, 2005; revised August 26, 2015.

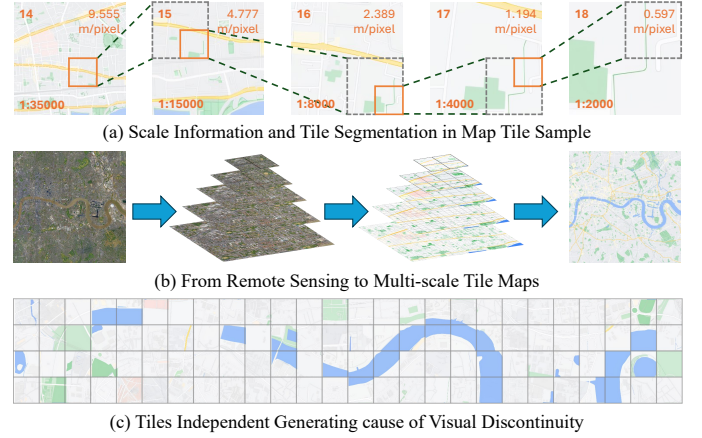


Fig. 1. The generation of multi-scale maps from remote-sensing images can leverage scale information and tile segmentation in multi-level tile map samples. However, independent tile generation may cause visual discontinuities in the generated map.

I. INTRODUCTION

MULTI-SCALE tile map services, admired for their accessibility and readability, play an essential role in modern society, with extensive applications in transportation, logistics planning, and personal navigation. Traditional cartography heavily depends on procuring and refining vector data, a labour-intensive and time-consuming process that hampers the ability to provide instantaneous map updates. This shortcoming becomes particularly critical in emergency scenarios, such as sudden geological disasters like earthquakes and mudslides, where the rapid generation of map tiles and immediate service updates are crucial. The advancements in remote-sensing technology now enable satellites, drones, and aircraft to swiftly capture high-resolution images rich in geographical information, making it feasible to generate map images directly from remote-sensing imagery.

Creating multi-scale tile maps using remote sensing imagery significantly reduces map production costs while exponentially enhancing the speed and efficiency of map updates (Fig.1(b)). Importantly, even in regions not easily accessible for on-site measurements, mapping technology that generates maps from remote sensing information provides an efficient, quick, and low-cost cartographic method.

Recent advancements in deep learning have significantly progressed image generation methodologies. Current techniques that leverage Generative Adversarial Networks (GANs)

[1], such as Pix2Pix [2], Pix2PixHD [3], and CycleGAN [4], facilitate domain shifts from remote sensing imagery to map tiles through the adversarial training of generators and discriminators. However, these approaches predominantly emphasize the intrinsic features of images while neglecting the relevance and complementarity of geographical features within remote sensing images, leading to maps that inadequately represent intricate geographical features. Various GAN-based map generation methods, such as GeoGAN [5], SMAPGAN [6], and CreativeGAN [7], have improved map generation effects to some extent. Nonetheless, these methods are confined to single-level map generation, employing single-level maps as samples during training and generation. The multi-level maps require training multiple models, thereby diminishing generation efficiency and limiting the model's generalization capability.

Several map generation methods, such as CscGAN [8] and LACG [9] generate multi-tier maps using fixed map level approaches. However, these methods overlook the extensive cartographic knowledge embedded in multi-level maps. They struggle to concurrently manage the challenges encountered in multi-level map generation, including significant scale variations, intricate details, and objective differences. Furthermore, the multi-level map generation process is vulnerable to information confusion and detail loss, adversely affecting the quality of the generated maps. Specifically, current map generation methods encounter the following principal challenges:

1) *Inadequate representation of complex geographical features*: Current map generation methods struggle to extract and represent intricate features. For example, surface elements such as buildings and vegetation are often omitted, while linear elements like roads and rivers may appear fragmented. The reliance on isolated geographical semantic extraction modules restricts the model's ability to fully understand the spatial context [7], thus impairing cross-modal spatial comprehension and reducing the generative model's expressive capabilities. Semantic segmentation samples can obscure detailed map information, affecting the generated maps' readability and consistency of style.

2) *Visual discontinuity in nearby generated map tiles*: WIn deep-learning-based map generation, constructing a cohesive map requires the integration of independently generated tiles (Fig.1(c)). These tiles, however, frequently exhibit visual discontinuities. Additionally, stylistic inconsistencies in geographic features across different tiles adversely affect the overall readability and aesthetics of the map. The lack of comprehensive geographical semantic information in tile samples further hinders the effectiveness of the training of the generative model.

3) *Inaccurate expression of scale in multilevel tile map*: Existing map generation models struggle to accurately express the cartographic synthesis characteristics of features at varying scales. Leveraging cartographic expert knowledge contained in extensive tile map samples (See Fig. 1(a)) to improve the accuracy of scale expression in generated maps presents a significant challenge. Current methodologies often link map levels to generated maps in a fixed manner [8], [9], failing to effectively integrate scale characteristics such as spatial

resolution, scale, and visual presentation. They neglect the comprehensive cartographic expertise embedded in multilevel maps, undermining the model's ability to express distinctive map scale features.

Recently, diffusion models [10], [11] have emerged as an innovative technology in image generation, demonstrating significant potential for producing high-quality images. These models generate images through a gradual denoising process and have shown superiority over GANs in handling complex scenarios and preserving details [12], [13]. The application of diffusion models in image generation tasks [14], [15] offers new insights into addressing the challenges of generating multi-level maps.

This paper introduces a multi-scale map generation method leveraging a conditional diffusion model to enhance the quality of multi-scale maps. It addresses challenges related to visual coherence, complex feature representation, and scaling accuracy in existing technologies. Unlike prior single-stage map generation methods, our self-cascaded map generation framework recursively produces multi-scale web maps from a given spatial scene. We develop a unified generation model that is applicable across various map scales. During each stage of map generation, variables such as the low-level map from the previous stage, map level, scale, and spatial resolution are integrated as controllable parameters to guide the creation of higher-scale, high-level map tiles. As the stages progress, the produced web maps exhibit diverse spatial resolutions, feature representations, and map syntheses, enabling the parallel generation of multi-level web map tiles for a given spatial scene.

Our specific contributions are as follows:

- 1) We devised a feature extraction network based on complementary feature learning. This innovative network efficiently extracts prior geographical information from the input remote sensing images, ensuring a rich representation of intricate geographical features in the resultant map.
- 2) We employed low-level map generation slices that aligned with the designated map generation range as spatial constraints and implemented a cascading generation strategy to produce large-scale network maps, progressing from low to high resolutions. This approach enables the generator to discern geographical features that span across tile map sheets from low-level map tiles, thereby ensuring stylistic and semantic coherence among the high-level map tiles generated.
- 3) We introduced a scale-modal information encoding mechanism based on the CLIP (Contrastive Language-Image Pre-training) model and constructed a fusion module utilizing SPADE (Spatially-Adaptive Normalization) for the prior remote sensing cartography features. This module adeptly integrates global and local content cues across various scales, ensuring that the generated map maintains consistency at all levels and accurately reflects the positioning of significant geographical elements.

To validate the effectiveness of our proposed method and address the limitations of existing datasets in multi-scale map cascade generation, we have constructed a real-world remote sensing image dataset from the Glasgow, UK. This dataset

achieves wide sample area coverage through coordinate sampling and selects continuous regional tile data from the London area to support continuous map range generation testing. The multi-level tile samples in the dataset facilitate the verification of cross-scale map cascade generation. The map scale information, such as map level, scale, and resolution associated with the remote sensing image-tile map sample pair, provides constraint information for multi-scale map generation.

The remainder of this paper is organized as follows: Section II reviews related work, while Section III outlines the main design and details of our approach. In Section IV, we introduce the collected CSCMG dataset and evaluate the performance of our approach on the multi-scale map generation task. Finally, conclusions are presented in Section V.

II. RELATED WORK

A. Traditional Cartography and Intelligent Interpretation

Currently, traditional mapping methods rely on data collection by professional surveyors and specialized software for subsequent processing. This results in a complex and resource-intensive production process. Regional and temporal limitations constrain these methods, and they exhibit low automation. In complex applications and urgent scenarios, these traditional methods often fail to respond rapidly to the requirements of map representation environments. They need to gain an efficient transition from basic data to thematic map products. As rapid urban construction transforms city landscapes, real-time map updates become essential. While major cities can update their maps within several months, updates for most small and medium-sized cities, as well as towns, can take up to a year [16], failing to meet the demands of rapid change. In particular, timely and accurate electronic map updates are crucial for emergency relief operations during sudden geological disasters. Therefore, there is an urgent need for a rapid and cost-effective map generation method to adapt to the ever-changing urban environment.

With the rapid advancement of remote sensing technology, capturing high-resolution remote sensing imagery has become increasingly effortless and efficient. This progress paves the way for adopting intelligent interpretation techniques based on deep learning, which inherently depend on high-quality data for optimal training. The primary tasks associated with the intelligent analysis of remote sensing imagery include semantic segmentation, feature object extraction, target detection, and scene classification. Remote sensing images are composed of many geographical elements, often intricate and diminutive, presenting notable challenges for their semantic segmentation. Existing methods for semantic segmentation in this domain have primarily focused on addressing these difficulties, particularly in the accurate segmentation of geographic elements within remote sensing imagery [17]–[28]. In terms of the pixel-level classification of land use and land cover within remote sensing imagery, significant attention has been devoted to challenges associated with the classification of large surface areas and heterogeneous land cover types [27], [29]–[35]. Similarly, research aimed at feature object extraction has explored methods to detect specific elements,

such as roads, by leveraging their geometric and topological characteristics for improved precision in extraction [36], [37]. For target detection, existing approaches tailored for remote sensing imagery have primarily concentrated on overcoming the challenges posed by detecting small, densely clustered objects, irrespective of their orientation or rotation [38]–[43]. Meanwhile, scene classification has increasingly integrated multimodal technologies, combining visual data from remote sensing imagery with geographical textual information. This synergy has given rise to foundational image-text models within the remote sensing field [44]–[48], establishing a robust framework for a wide range of downstream applications.

The intelligent interpretation of remote sensing imagery provides a wealth of geographic information, serving as a vital resource for cartographic endeavors. Pre-trained foundational models for remote sensing imagery offer a powerful and reliable mechanism for feature extraction in map-making processes. Furthermore, certain map generation methods leveraging remote sensing imagery [5]–[8], [49]–[51] have significantly streamlined and accelerated the production of maps, rendering the process more efficient and accessible.

B. Map Generation Methods Based on GAN Model

Map generation represents a crucial application of image-to-image translation, aiming to transform remote sensing imagery into interpretable and visually harmonious maps. However, the pronounced domain gap between remote sensing imagery and map representations introduces notable challenges, demanding careful refinement to enhance the quality of the generated outputs. Although traditional GAN-based methods for image generation, such as Pix2Pix [2], Pix2PixHD [3], and CycleGAN [4], have been applied to image-to-image translation tasks, they are not specifically designed to address the inherent complexities of converting remote sensing data into maps. Consequently, these approaches frequently fail to adequately extract and represent the intricate features of objects in remote sensing imagery, resulting in maps of subpar quality compared to those produced by methods specifically tailored for this domain.

Researchers have developed specialized techniques to generate maps from remote sensing imagery. For instance, GeoGAN [5] employs a Conditional Generative Adversarial Network (cGAN) [3] to translate remote sensing imagery into map representations, while SMAPGAN [6], a semi-supervised generative model, leverages incompletely paired remote sensing and internet map sample data to produce maps, although it does not fully overcome the issue of map quality. Additionally, Fu et al.'s CreativeGAN [7] incorporates semantic information to improve the accuracy of generated maps. These GAN-based methodologies refine the outputs through adversarial training dynamics between generators and discriminators, where discriminators assess image authenticity and penalize deviations from the target appearance. However, these methods predominantly focus on single-level map generation and fail to accommodate the intricate requirements of multi-scale map generation.

To tackle the specific challenges associated with multi-scale map generation, Chen et al. [52] proposed a straightforward

training approach for producing hierarchical maps. At the highest level (k -th level, where k denotes the maximum scale), this strategy generates maps directly from remote sensing imagery, whereas at lower levels, the mappings between the k -th and $(k - 1)$ -th levels are learned through independently trained models. However, this approach exhibits notable limitations: the training process is complex, as each level requires a distinct model, and the accuracy of the highest-level map constrains the quality of lower-level maps. This results in insufficient utilization of the features within remote sensing imagery. In contrast, Liu et al. [8] developed a multi-level map generation network capable of producing multi-level maps using a single model. This approach introduces a map-level classifier, inspired by StarGAN [53], as an extension to the discriminator.

Additionally, it utilizes preprocessed road morphology data as input. Nevertheless, this method struggles to generate consistent multi-level maps solely from remote sensing imagery, as its multi-level maps pertain to disparate regions rather than representing varying scales of the same area. This limitation narrows its applicability for multi-level map generation within a cohesive geographic region. Fu et al. [9] addressed this gap by employing a level classifier to distinguish and generate map tiles across different levels. Their network introduces a map element extractor to capture significant geographic features from satellite imagery and incorporates a multi-level fusion generator to produce seamless multi-level maps from initial lower-level map inputs. However, their architecture relies on independently generated map tiles, which, when assembled, often exhibit visual discontinuities that detract from the overall readability and aesthetic coherence of the resulting map.

In conclusion, existing methodologies for map generation tend to focus on either single-level maps or fail to meet the demands of generating consistent multi-scale maps within a unified geographic region. In light of these limitations, an end-to-end generative approach for cartography was proposed, specifically designed to produce high-quality, seamless, and wide-area multi-scale web maps from remote sensing imagery. This method addresses the challenges inherent in multi-scale map generation, ensuring enhanced consistency and usability for regional map production.

C. High-resolution Image Generation using Diffusion Model

Drawing inspiration from thermodynamics, diffusion models iteratively introduce noise, striving to capture and learn the patterns of informational decay induced by noise, thereby enabling the generation of images based on these learned dynamics [54]. These models have demonstrated exceptional performance in high-resolution image generation tasks. Among them, the Denoising Diffusion Probabilistic Model (DDPM) [10] stands as a prominent representative in the field. DDPM functions by reversing the diffusion process: during the forward process, noise is progressively added to the original data until it transforms into Gaussian noise. The model is trained to reverse this process step-by-step, reconstructing data from noise. Building upon this foundation, Nichol et al. [55] introduced a learning variance strategy within DDPM,

significantly enhancing the quality of synthesized images while simultaneously improving the speed of the sampling process. To further expedite sampling, Song et al. proposed the Denoising Diffusion Implicit Model (DDIM) [11], which reformulated the diffusion process as non-Markovian. Without altering DDPM's training methodology, the DDIM framework substantially boosted sampling speed while maintaining near-identical image generation quality. Furthermore, DDIM established a deterministic generation process, ensuring that the resulting images were solely influenced by the initial noise used in the reverse process.

The diffusion models are primarily unconditional generation models, producing images through random sampling without relying on external controls. On the other hand, conditional diffusion models generate images by incorporating additional control signals. Such models allow for the integration of diverse input conditions, spanning classification-to-image generation [56], image-to-image synthesis [14], [57], [58], text-to-image generation [59]–[61], and image editing [62]–[65], among others. However, as DDPM's reverse process operates directly in pixel space, predicting high-dimensional noise demands substantial computational resources and memory, posing challenges for high-resolution image generation. Two principal strategies have been devised to surmount this limitation: cascade generation [56], [60], which begins with the generation of a low-resolution image and progressively synthesizes higher-resolution images by treating the preceding stages as conditional inputs; and latent space generation [59], which compresses the image into a lower-dimensional latent space using an encoder-decoder framework and performs the denoising diffusion process within this latent space. Both approaches have proven effective in optimizing the efficiency of high-resolution image synthesis using diffusion models.

Inspired by the aforementioned excellent works, we proposed a cascade diffusion generation strategy and an innovative approach tailored for multi-scale map generation. Traditional map generation models demand the design and training of separate models for each scale stage, thereby inflating training costs. In contrast, our model employs shared network weights across all stages while leveraging encoded multi-scale map information to guide the learning of map synthesis. This approach reduces training complexity and costs and expands the learning capacity, offering a more robust framework for multi-scale map generation.

III. METHOD

A. Overall Framework

We propose a novel self-cascading generative mapping framework, named **Cascading Conditional Generative Mapping framework (C2GM)**, designed to generate tile maps across diverse scales. As depicted in Fig. 2, the overarching design of C2GM enables the recursive reconstruction of large-scale tile map using a unified generative model.

The generation process is structured into sequential stages, starting with the synthesis of lower-level maps and progressively creating higher-level ones. The model incorporates three key inputs at each generative stage: remote sensing images,

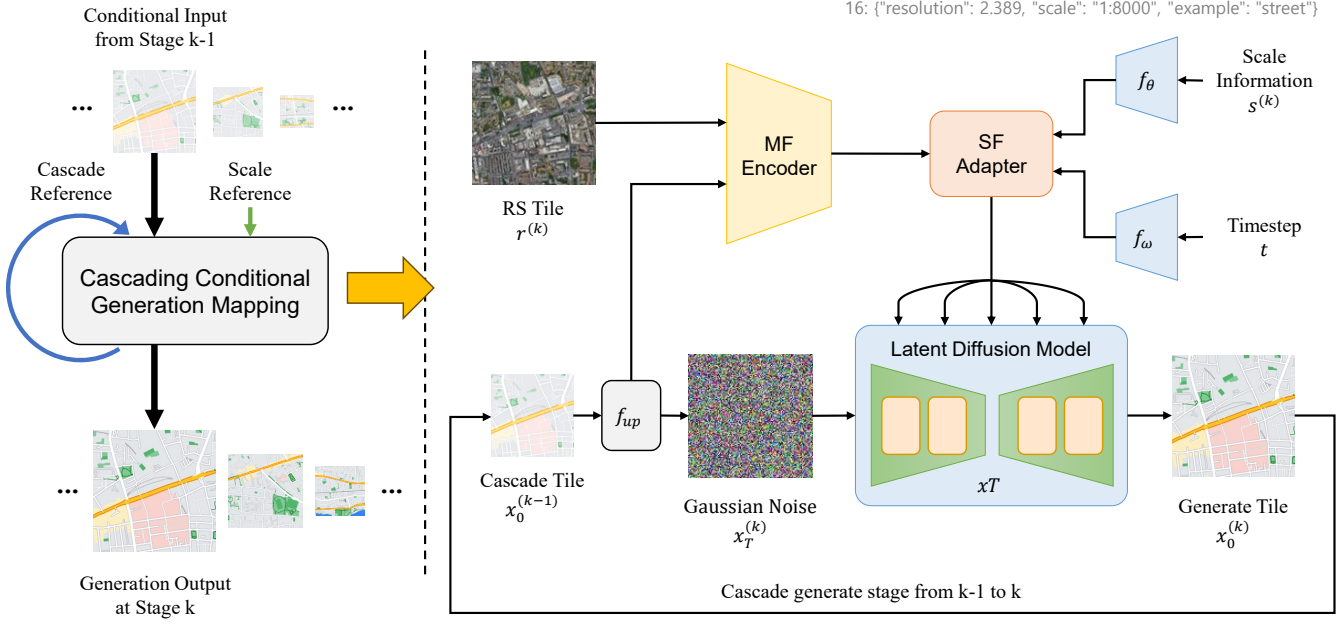


Fig. 2. The overall structure of C2GM encapsulates a hierarchical, self-cascading design aimed at producing multi-scale, large-area tile maps for specified spatial scenarios. The generation process is divided into multiple stages, starting with lower-level maps and gradually transitioning to higher-level ones. In each stage, the generation process depends on the lower-level tile previously produced and its scale information. This multi-stage generation strategy not only enhances the quality of map tile generation but also ensures consistency and coherence across different tiles by learning the disparities between various map scales and integrating cartography expertise.

cascading references, and corresponding scale information. Remote sensing images provide essential geo-object features for cartographic synthesis; lower-level map tiles serve as cascading references, offering pre-existing cartographic characteristics to guide the generation process; and scale information enables the model to adapt to and represent map features at various scales.

At the k th generation stage, let $x_0^{(k)}$ denote the target map and $s^{(k)}$ represent the scale information, encompassing elements such as map layer $s_z^{(k)}$, spatial resolution $s_r^{(k)}$, scale ratio $s_s^{(k)}$, and geospatial representation $s_f^{(k)}$. When generating the map for the $(k+1)$ th stage, the input conditional variables $x_0^{(k)}$ and $s^{(k)}$ are embedded into the model. Assuming that during each stage, the model increases the tile level $s_z^{(k)}$ of the input tile by n levels (e.g., $n = 1$), and if the map tile size generated at the k th stage is $H \times W$ pixels, the $(k+1)$ th stage output will comprise 4^n map tiles at level $s_z^{(k)} + n$. These new tiles correspond to the geographic area covered by the k th stage tile but are represented within a frame of $2^n \cdot H \times 2^n \cdot W$ pixels.

Through a parallel generation mechanism, the above operation can be iteratively repeated m times, starting from the k th stage, eventually resulting in a full tile map consisting of multiple layers and scales. Formally, the resulting tile map can be expressed as:

$$\mathcal{X} = \{x_0^{(k)}, x_0^{(k+1)}, \dots, x_0^{(k+m)}\},$$

where the tile map produced at the $(k+m)$ th stage, $x_0^{(k+m)}$, corresponds to the map layer $s_z^{(k)} + m \cdot n$ and has an ultimate size of $H \cdot 2^{(n \cdot m)} \times W \cdot 2^{(n \cdot m)}$ pixels.

B. Conditional Denoising in Map Generation

The Denoising Diffusion Probabilistic Models (DDPMs) represent a class of advanced generative models rooted in the principles of the diffusion process. The fundamental mechanism of DDPMs involves the gradual addition and subsequent removal of noise, simulating a diffusion-like transformation of data to generate new samples [10]. These two phases—forward diffusion and reverse denoising—correspond to the training and sampling stages of the model, respectively. The traditional DDPM conducts both the forward and reverse processes directly over the entire pixel space, with the diffusion process mathematically described as follows:

$$y_t = \sqrt{\bar{\alpha}_t} y_0 + \sqrt{1 - \bar{\alpha}_t} \epsilon, \quad \epsilon \sim N(0, 1) \quad (1)$$

where y_0 denotes the data sampled from the true data distribution, and $\bar{\alpha}_t$ represents a predefined hyperparameter governing the noise schedule. The term ϵ corresponds to random noise drawn from the standard Gaussian distribution. The DDPM framework centers on training a denoising function ϵ_θ , which estimates the noise component embedded in y_t , constrained by an L_2 loss function:

$$L = \mathbb{E}_{(y_0, \epsilon, t)} \|\epsilon - \epsilon_\theta(y_t, t)\|^2 \quad (2)$$

In this equation, t denotes an integer time step drawn from the interval $[0, T]$, while ϵ_θ signifies the noise predictor that undergoes training. Minimizing the aforementioned loss function allows the model to progressively transform random noise into high-quality data throughout the reverse denoising procedure. For more precise and controlled data generation, supplementary conditioning variables can be integrated into the noise predictor, yielding an extended formulation such as

$\epsilon_\theta(y_t, t, c)$, where c encapsulates the conditioning information. Based on the underlying principles of DDPM, each incremental step within the denoising operation can be mathematically formulated as follows:

$$y_{t-1} = \frac{1}{\sqrt{\alpha_t}}(y_t - \frac{\beta_t}{\sqrt{1-\alpha_t}}\epsilon_\theta) + \sigma_t\epsilon, \quad \epsilon \sim N(0, 1) \quad (3)$$

where α_t , $\bar{\alpha}_t$, β_t , and σ_t are predefined hyperparameters governing the noise schedule, and ϵ denotes additional noise injected during the reverse process. After $T-1$ iterations, this method yields a final sample conditioned on c .

Despite their high-quality results, DDPMs are computationally intensive and time-consuming for training and inference, making them less practical for certain applications. Addressing this limitation, Latent Diffusion Models shift the diffusion and denoising processes from pixel space to a lower-dimensional latent space learned by a pre-trained autoencoder. This paradigm drastically reduces the dimensional complexity while maintaining crucial data details. The encoding and decoding operations of the autoencoder can be defined as follows:

$$z_0 = \mathcal{E}(y) \quad (4)$$

$$y \approx \mathcal{D}(z_0) \quad (5)$$

where z_0 denotes the latent representation of the target data y , \mathcal{E} represents the encoder, and \mathcal{D} is the decoder, both of which are pre-trained. As a result, the entire diffusion and denoising processes are executed in the latent space, where z_0 resides. This design achieves an optimal balance between computational efficiency and the preservation of data fidelity.

Map generation models rely solely on remote sensing imagery tiles as inputs to produce corresponding spatial scene map tiles. This process can be mathematically expressed as follows:

$$y = \arg \min_y -\log(p(y|x)) \quad (6)$$

where x denotes the remote sensing imagery tiles, while y represents the generated map tiles. The term $p(\cdot|x)$ refers to the conditional probability density function of the target map given the remote sensing imagery input, typically modeled as either a standard Gaussian distribution (L_2 loss) or a Laplacian distribution (L_1 loss), with the true target map serving as its mean. This approach, which relies exclusively on remote sensing imagery tiles, theoretically learns the many-to-one mapping between remote sensing tiles and the corresponding map tiles. However, when applied to multi-scale map generation, these methods often need to be revised, struggling to extract precise semantic information about geo-objects across multiple scales of remote sensing imagery.

To address these limitations, drawing inspiration from advancements in decoupled feature learning, we propose the following revised modeling approach:

$$y = \arg \min_y -\log(p(y|x, con, rsm)) \quad (7)$$

where con and rsm represent scale information and cascading reference conditions. Both serve as pivotal components for encoding map scale information. In the context of this methodology, the terms are defined as follows:

- **Scale Information:** The cross-modal constraints of scale features correspond to the map's level. These encapsulate the spatial resolution, scale, and textual representation of geographic objects associated with the specified level of the generated map.
- **Cascade Reference:** The visual representation of map sheets and geographic object information from lower levels, acts as cascading feature constraints.

During the training phase, any useful prior knowledge can be utilized to provide content guidance. In the testing phase, multi-scale reconstruction results are derived using scale information and cascading reference. By decomposing cartographic reference information into scale and cascading features, this modeling approach enables improved reconstruction guidance, delivering higher-quality generation results with enhanced scale representation and stronger semantic fidelity.

C. Scale-Guided Diffusion Model

Considering the complexities introduced by large-scale factors in the super-resolution of remotely sensed images in real-world scenarios, we present an innovative scale-unified map generation model named the **Scale-guided Diffusion Model (SGDM)**. Remarkably, in contrast to previous single-image map generation models, SGDM can simultaneously process input from remote sensing image tiles, target map tiles, and cascading reference tiles. This synergy facilitates the generation of map tiles tailored to specific levels (scales). The core architecture of SGDM is illustrated in Fig. 3. The SGDM framework is composed of four integral components: the pre-trained Variational Auto-Encoder (VAE), the denoising U-shaped network (U-Net) with skip connections, the Map Feature Encoder (MFEncoder), and the Scale Feature Adapter (SFAdapter). The VAE encodes and decodes high-resolution (HR) images, thereby transitioning the conventional DDPM diffusion and denoising process from pixel space to latent space, enhancing training stability and reducing computational overhead. Concurrently, the U-Net, functioning as a conditioned noise predictor, iteratively predicts and removes noise to achieve clean data. It is constructed with multiple encoding, middle, and decoding layers, most of which are composed of residual blocks, cross-attention, and self-attention modules. The MFEncoder integrates prior information from the style guide map, remote sensing image, and scale reference map to produce a conditional feature map enriched with semantic and stylistic details. Finally, the Scale Feature Adapter (SFAdapter) converts these conditional features into multi-scale features (about the image domain scale rather than the geographic domain scale) that are compatible with the U-Net architecture. These features are incorporated into the outputs of the U-Net's encoding and decoding layers on an element-wise basis, ensuring seamless feature integration and effective guidance throughout the generation process.

1) *Scale Information Guidance:* At each generation stage, the previously generated lower-level tiles, along with time step and scale information embeddings are utilized as conditional input variables. For the lower-level tile input — cascading reference map $x_0^{(k)}$ — its dimensions do not align with $x_t^{(k+1)}$.

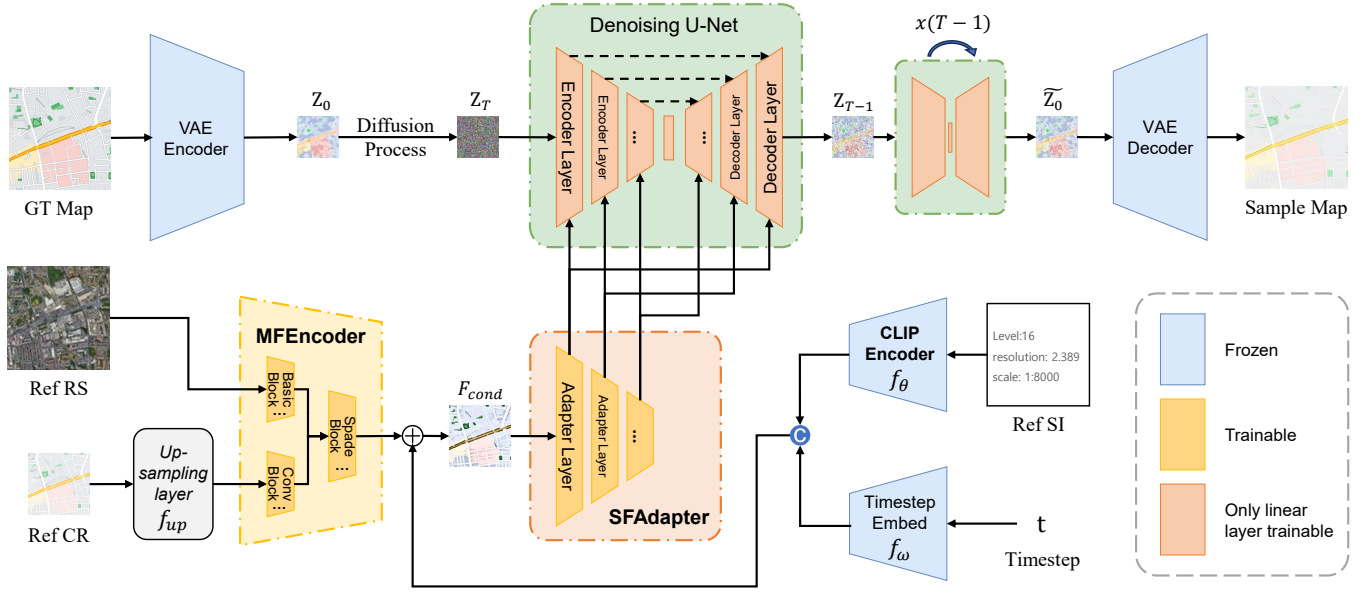


Fig. 3. The SGDM architecture leverages a Variational Autoencoder (VAE) to transition the diffusion and reverse processes from pixel space to latent space. During training, the latent representation of the target map, z_0 , undergoes a progressive transformation into z_t through the diffusion process, followed by denoising achieved via a U-Net network. Two bespoke modules are introduced to further refine the denoising process: the Map Feature Encoder (MFEncoder) and the Scale Feature Adapter (SFAdapter). The MFEncoder integrates information derived from remote sensing imagery and cascading references to construct the conditional feature, F_{cond} . Expanding on F_{cond} , the SFAdapter produces multi-scale features that are subsequently merged with the outputs of corresponding U-Net layers through element-wise addition.

To address this, and inspired by [57] and [66], we redesigned the network architecture. First, as illustrated in Fig. 3, the encoder E_{lr} is applied to encode the lower-level map tiles $x_0^{(k)}$. Then, a series of upsampling and convolutional layers f_{up} are employed to align the feature map dimensions with $x_t^{(k+1)}$. Finally, the features are fused by concatenating $x_t^{(k+1)}$ and the feature maps along the channel dimension:

$$\tilde{x}_t^{(k+1)} = \text{cat}[x_t^{(k+1)}, f_{up}(E_{lr}(x_0^{(k)}))] \quad (8)$$

where $\text{cat}(\cdot)$ represents the concatenation operation along the channel dimension.

For the scale information s in text modality data, we perform cross-modal encoding using pre-trained CLIP model [67], [68], with the CLIP scale encoder denoted as f_θ (Fig. 3). This approach allows us to obtain the embedding vector of scale information $e_s^{(k)} = f_\theta(s)$ at each generation stage, capturing the cross-modal representation of scale information corresponding to the spatial context of the generated map. This embedding subsequently guides the map generation process through the cross-attention mechanism [69] during denoising:

$$e_s^{(k)} = f_\theta(s_z^{(k)} + s_r^{(k)} + s_s^{(k)} + s_f^{(k)}) \quad (9)$$

Through this process, the scale information embedding $e_s^{(k)} \in \mathbb{R}^D$ is obtained at the k -th generation stage. The time step variable $t \in \{1, \dots, T\}$ is then encoded via a frequency encoding transformation f_ω :

$$e_t = f_\omega(t) \quad (10)$$

Here, θ_t is a learnable parameter.

Finally, $e_s^{(k)}$ and e_t are combined to generate the final conditional embedding vector for the k -th generation stage and the t -th denoising step:

$$e_t^{(k)} = e_s^{(k)} + e_t \quad (11)$$

Using the conditional embedding vector $e_t^{(k)}$ and the cascade map feature $\tilde{x}_t^{(k)}$, we define the conditional variable for the k -th generation stage and t -th denoising step as:

$$c_t^{(k)} = \{e_t^{(k)}, \tilde{x}_t^{(k)}\} \quad (12)$$

This condition $c = c_t^{(k)}$ is then used as input to model the following conditional probability density function $p_\theta(y | x, c)$:

$$p_\theta(x_{0:T} | c_t^{(k)}) = p(x_T) \prod_{t=1}^T p_\theta(x_{t-1} | x_t, c_t^{(k)}) \quad (13)$$

$$p_\theta(x_{t-1} | x_t, c_t^{(k)}) = \mathcal{N}(x_{t-1}; \mu_\theta(x_t, t, c_t^{(k)}), \sigma_t^2 I) \quad (14)$$

Based on (7), while keeping the forward process unchanged, we construct a conditional denoising model:

$$y = \arg \min_y -\log(p_\theta(x|c)) \quad (15)$$

Through this design, we can ultimately generate map tiles of varying scales in a self-cascading manner, encoded with information on resolution, temporal steps, and scale.

2) *Map Feature Encoder*: To facilitate the successful amalgamation of cascading information from cascading reference tiles into remote sensing image tiles, we have developed a multi-branched map feature encoder (MFEncoder), illustrated in Fig. 3. This encoder integrates semantic information from cascading reference tiles into remote sensing image tiles across various scales. As illustrated in Fig. 4(a) convolutional and

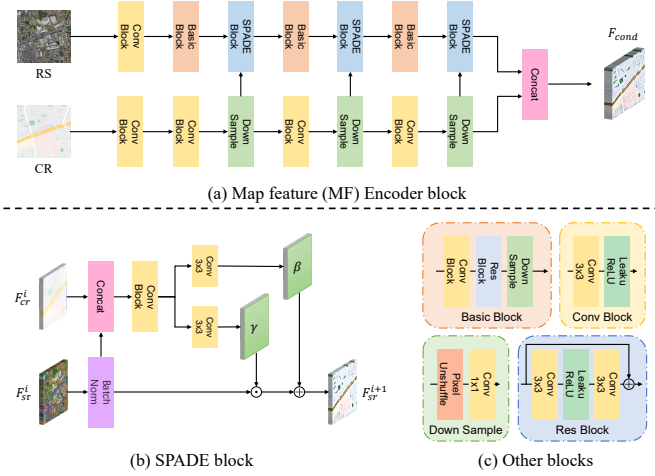


Fig. 4. Detailed structure of the proposed Multi-branch Mapping Feature Encoder (MFEncoder): it can generate the conditioned features F_{cond} that contain cartographic semantic information by utilizing the content information of the reference map at multiple scales through the SPADE module.

down-sampling blocks are employed in one branch to extract multi-scale features from the cascading reference tiles. The multi-scale features are derived from the remote sensing image tiles through the Basic Block in another branch. To achieve the fusion of these features, we have incorporated the SPADE (Spatially-Adaptive Normalization) module at each scale. In our design, the input to the SPADE block comprises feature maps from remote sensing image tiles, abundant in coarse texture and structural information. As illustrated in Fig. 4(b), our enhanced SPADE module distinguishes itself from the original design by utilizing features from both remote sensing and cascading reference tiles to compute the scaling factor γ and the offset term β . This approach enables a flexible and high-fidelity integration of content-guided information into the features of remote sensing images. The entire process is detailed as follows:

3) *Scale Feature Adapter*: The MFEncoder excels in integrating texture and structural features from remote sensing image tiles, alongside content features from cascading reference tiles, ultimately producing the conditional feature F_{cond} . Given that F_{cond} encompasses the majority of external information requisite for map generation, the function of the Scale Feature Adapter (SFAdapter), illustrated in Fig. 3, is primarily to generate multi-scale features and align them with the pre-existing knowledge of the pre-trained stable diffusion model.

Consequently, the architecture of the SFAdapter module is inherently straightforward, primarily comprising stacked convolutional layers, residual blocks, and down-sampling blocks (Fig. 4(c)). The SFAdapter module progressively increases the channel count of the feature maps while simultaneously diminishing their spatial dimensions, resulting in three distinct sets of conditional features. These features are then integrated into the output of the U-Net network layer by layer, on an element-wise basis, to facilitate the generation process of the stable diffusion model.

D. Loss Function

As illustrated in Fig. 3, the trainable parameters of the Scale-Guided Diffusion Model (SGDM) are determined by the following loss function:

$$L = \mathbb{E}_{(z_0, \epsilon, rs, cr, t)} \| \epsilon - \epsilon_\theta(z_t, t, rs, cr) \|^2 \quad (16)$$

This equation, rs and cr , represents the input remote sensing image tiles and cascading reference tiles. Here, ϵ denotes randomly sampled Gaussian noise, while t signifies the integer timestamp sampled from the interval $[0, T]$. In this context, ϵ_θ refers to the denoising U-Net model.

IV. EXPERIMENT

A. Experimental Setup

1) *Datasets*: In this pursuit, we have established a novel benchmark dataset called the Cross-Scale Cascade Map Generation Dataset (CSCMG) to validate the proposed C2GM framework and stimulate future research in large-scale remote sensing image super-resolution. The data were meticulously collected from the Glasgow area in the UK, ensuring that the sampling regions for the test and training tile sets were distinctly delineated and non-overlapping. Representative image pairs are illustrated in Fig. 5.

TABLE I
DETAILED INFORMATION FOR THE CSCMG DATASET.

| Level | Tile pair number | | Scale | Resolution (m/pixel) | Example features |
|-------|------------------|-------------|---------|----------------------|------------------------|
| | Training set | Testing set | | | |
| 14 | 4870 | 280 | 1:35000 | 9.555 | village, or suburb |
| 15 | 15106 | 292 | 1:15000 | 4.777 | small road |
| 16 | 30040 | 300 | 1:8000 | 2.389 | street |
| 17 | 40555 | 300 | 1:4000 | 1.194 | block, park, addresses |
| 18 | 45000 | 300 | 1:2000 | 0.597 | some buildings, trees |
| All | 135571 | 1471 | - | - | - |

CSCMG comprises pairs of remote sensing and map tiles across various scales, ranging from levels 14 to 18, as detailed in Table I. The dataset includes 137,042 sample tiles, with 135,571 allocated for training and 1,471 designated for testing. All tiles were sourced from Google Maps' free tile service. The extensive multi-level tile samples within the dataset enable robust validation of multi-scale map generation capabilities.

Tiles span from level 18 down to level 14, encompassing the entire spatial extent of all sub-level tiles structured through a quadtree division. This design enhances both the training and testing processes of the cascade map generation model. The dataset offers cascade training data at 2X and 4X, providing cascading references covering either one or two levels. As illustrated in Fig. 6, the image resolutions of the reference tiles are either 128 or 64, upscaled to 256 to ensure uniform tile sizes while preserving the spatial resolution of the original references. This approach facilitates the validation of the efficacy of multi-scale cascading generation. Bi-cubic resampling is employed to maintain a 2X or 4X spatial resolution difference between the map tiles and cascading reference tiles.

To evaluate our method's multi-scale map generation capabilities, we utilize the multi-scale map generation dataset MLMG constructed by the state-of-the-art (SOTA) method LACG [9]. The MLMG dataset assesses multi-scale map

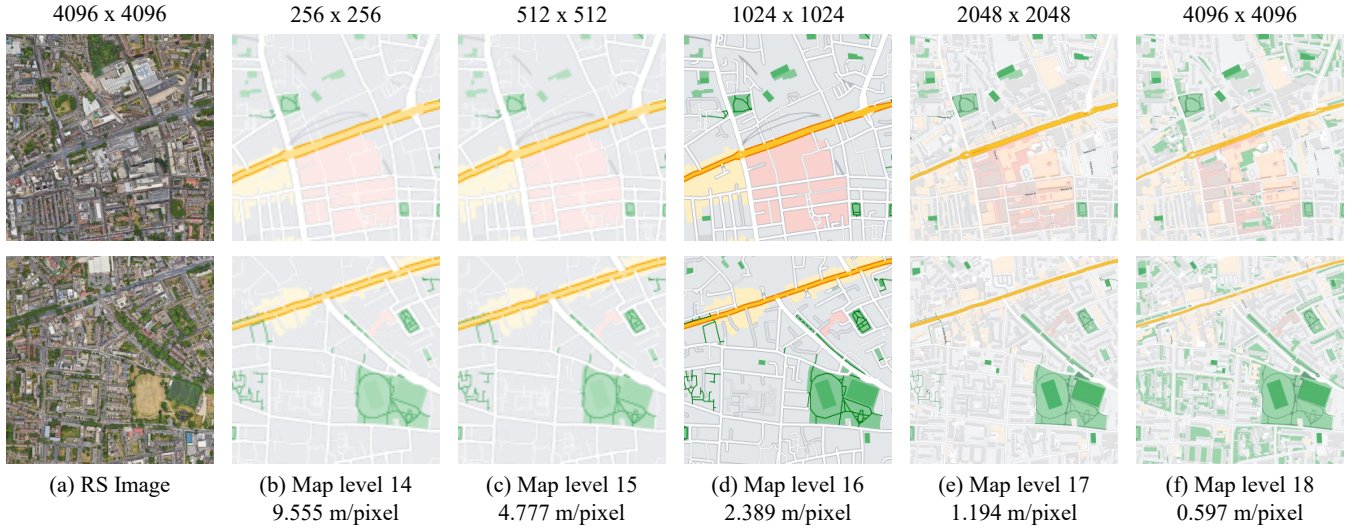


Fig. 5. Examples of RS-Map tile sample pairs from levels 14 to 18 in the CSCMG dataset are provided. The dataset covers a broad range of cross-scale scenarios, including forests, rivers, streets, residential areas, industrial areas, bodies of water, plazas, and more.

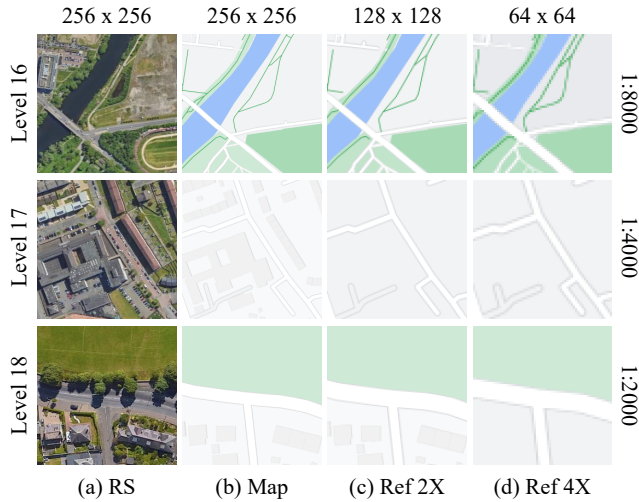


Fig. 6. Examples of cascade references from levels 16 to 18 in the CSCMG dataset. The dataset provides 2X or 4X cascade references, with image resolutions of 128 and 64.

generation techniques and includes tiles from diverse urban environments such as forests, rivers, streets, residential areas, industrial zones, water bodies, and squares. The dataset comprises samples collected from cities in the United States and China, reflecting significant differences in their respective images and maps. In China, roads are typically wider with lower distribution density, lacking a clear parallel-vertical relationship, whereas in the United States, roads are generally straight and densely packed, with the ground neatly segmented into blocks. The dataset from the U.S. city is MLMG-US, while the dataset from the Chinese city is MLMG-CN. Both MLMG-US and MLMG-CN contain equal samples and levels, featuring multi-scale remote sensing images paired with corresponding map tiles and element labels.

2) *Evaluation Metrics*: We utilize image quality evaluation metrics to comprehensively assess the performance of various remote sensing image super-resolution methods. The realism

of the generated maps is quantified through the Peak Signal-to-Noise Ratio (PSNR) and Structural Similarity Index Measure (SSIM), both computed on the Y channel within the YCbCr color space [70]. Additionally, the Fréchet Inception Distance (FID) is employed to evaluate the divergence in distribution between real and generated maps [71].

3) *Implementation Details*: Our proposed C2GM framework is based on the Stable Diffusion 2.1-base model. The SGDM model is implemented using the PyTorch framework, and all experiments are conducted on two NVIDIA GeForce RTX 3090 GPUs. The training process leverages cascaded map tiles spanning levels 14 to 18 from the CSCMG dataset.

The training procedure is divided into two distinct stages. The Stable Diffusion model is fine-tuned in the first stage using the loss function defined in Section III-D. During this phase, the parameters of the Map Feature Encoder (MFEncoder), Scale Feature Adapter (SFAdapter), and the linear layers of the U-Net are optimized. The model comprises 152 million trainable parameters, with a total size of 1.4 billion. Training is carried out for 200,000 steps with a batch size of 20, utilizing the AdamW optimizer and setting the learning rate to 5×10^{-5} .

B. Experimental Results

To substantiate the efficacy of our technique, we compared our method against established image-to-image conversion methods (Pix2pix [2], Pix2pixHD [3], CycleGAN [4], SPADE [72]), map generation techniques grounded in remote sensing imagery (SMAPGAN [6], Creative GAN [7]), and the current state-of-the-art map generation method, LACG [9].

1) *Quantitative Evaluation*: We employed the MLMG to evaluate these models individually, with the results presented in Table II. Regarding the FID and PSNR metrics, our method consistently achieved optimal outcomes on average. Specifically, on the MLMG-CN dataset, the proposed method recorded an FID index of 103.99 and a PSNR index of 29.759, outperforming other methods. Similarly, the MLMG-US dataset achieved an FID index of 104.63 and a PSNR

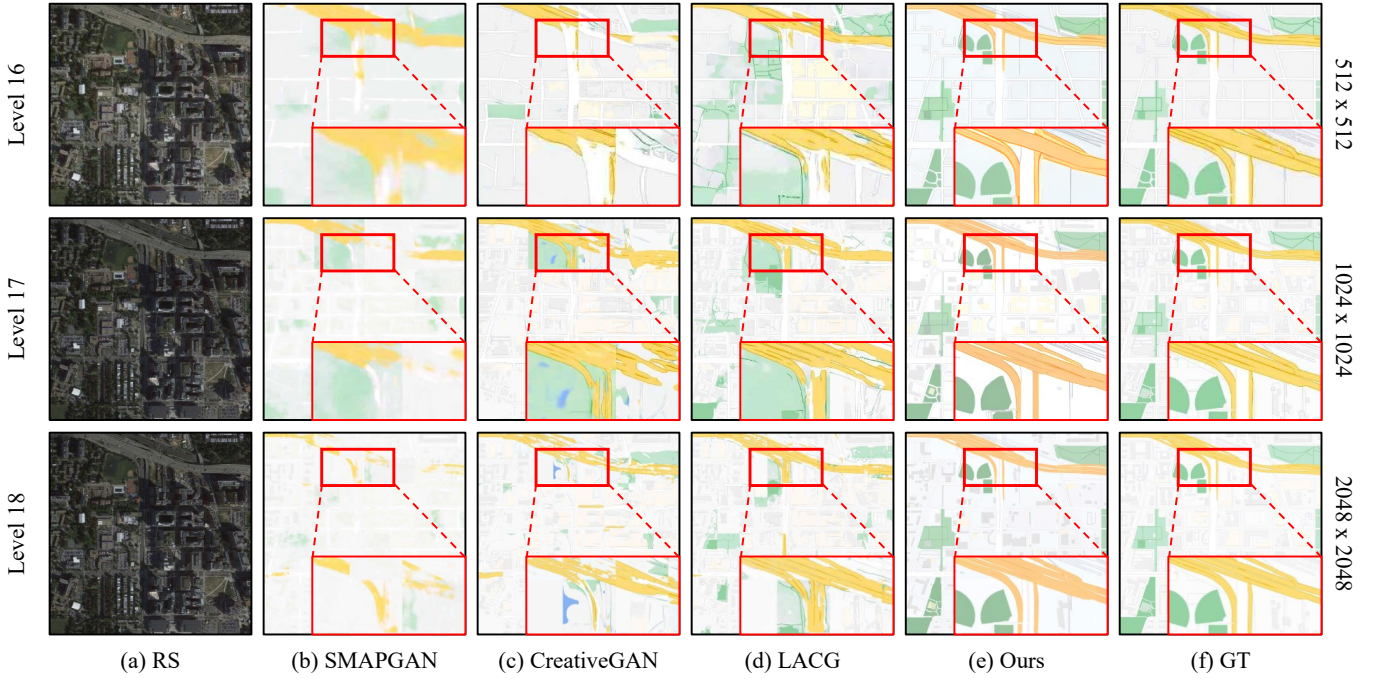


Fig. 7. Visualized results of map generation on the MLMG-US test set using our method and analogous approaches are presented. However, due to the limitation of reference information, only the results for levels 17 and 18 are available in section (k) of the figure. Our results demonstrate superior accuracy in map scale representation and enhanced visual continuity of the combined tile map.

index of 28.012, demonstrating superior performance. These results indicate that our method surpasses others in these image quality evaluation metrics, effectively validating its efficacy. Notably, the FID results highlight a significant advantage, suggesting that the distribution difference between the maps generated by our method and the real maps is minimal, thus reflecting high-quality output.

Furthermore, we identified suboptimal results in the testing outcomes; for instance, the LCAG method exhibited a suboptimal performance in the FID metric, underscoring the substantial advantage of our method in terms of perceived quality compared to LCAG. In the context of the PSNR metric, our method outperformed the suboptimal SMAPGAN method, indicating higher similarity in the generated maps. However, it is important to note that some researchers have pointed out that a higher PSNR does not necessarily correlate with improved visual quality [73], [74]. We opted to retain this metric as it provides a relative measure of the generated map quality across different methods and is a valuable reference in ablation studies.

We attribute the discrepancies observed in test results between the MLMG-CN and MLMG-US datasets to the inherent differences in the datasets themselves. The MLMG-CN dataset is derived from map data of Chinese cities, while the MLMG-US dataset is based on American city map data. The geographic information within these two datasets varies significantly, resulting in differing test outcomes. Notably, the map data from American cities may exhibit more complex geographic features, whereas the ground features in Chinese cities tend to be more regular, contributing to the lower performance observed in the MLMG-US dataset compared to the MLMG-CN dataset.

TABLE II
QUANTITATIVE COMPARISON OF DISPARATE
METHODOLOGIES ON THE MLMG DATASET.

| Model | MLMG-CN | | MLMG-UN | |
|--------------|---------------|---------------|---------------|---------------|
| | FID↓ | PSNR↑ | FID↓ | PSNR↑ |
| Pix2Pix | 227.31 | 23.16 | 248.66 | 26.406 |
| Pix2PixHD | 195.48 | 23.044 | 188.22 | 25.297 |
| CycleGAN | 213.99 | 22.515 | 153 | 24.85 |
| SPADE | 332.78 | 23.166 | 304.46 | 25.948 |
| SelectionGAN | 261.07 | 23.169 | 260.18 | 25.563 |
| SMAPGAN | 290.65 | <u>24.918</u> | 347.38 | <u>27.564</u> |
| CreativeGAN | 172.74 | 23.204 | 149.34 | 25.683 |
| LCAG | <u>134.05</u> | 23.876 | <u>125.8</u> | 25.409 |
| C2GM-2X | 114.21 | 29.204 | 124.46 | 27.318 |
| C2GM-4X | 103.99 | 29.759 | 104.63 | 28.012 |

2) *Qualitative Evaluation:* We conducted a visual comparison with all comparative models. Fig. 7 shows that most methods have difficulty generating accurate and continuous cartographic features, such as roads, buildings, and vegetation. We find that multi-level results from single-scale methods exhibit more ground object errors, feature breaks, and discontinuous tile noise, particularly at higher levels. Map generation methods designed for multi-level map generation, such as SMAPGAN, CreativeGAN, and the SOTA method LCAG, perform well in multi-level scale expression. However, their tile results have obvious visual discontinuity problems after map splicing, and the features of the objects they express also have fractures and noise. Compared with other methods, our proposed method is significantly better in terms of the integrity of geographical features and the visual continuity of map tiles. Our method is closer to the ground truth (GT) than other methods, especially in the high-level tile map generation results.



Fig. 8. Visual results of the ablation study on the CSCMG dataset are presented. Results of our method are visualized after incrementally adding modules. These results demonstrate that the proposed method can generate high-quality and continuous tile maps with the assistance of the cascade reference (MFEncoder) and scale information reference (CLIPEncoder).

Vertical comparison of the generation outcomes at different levels reveals that other methods produce similar ground object representations, highlighting a problem of inconsistency between map synthesis and map scale. In contrast, the maps generated by our proposed method demonstrate superior synthesis features across various levels. For instance, in the 18-level and 16-level maps, our method showcases more pronounced differences in ground object representation compared to other methods, effectively conveying more accurate map synthesis scale information. These results underscore that our method significantly outperforms the comparison methods in generating multi-scale maps from remote sensing imagery, thereby validating the effectiveness of our approach.

C. Ablation Studies

The ablation experiments are divided into two parts. Experiment 1 investigates the impact of incorporating scale information (CLIPEncoder) into the Baseline, illustrating how scale information guidance affects the generated map. Experiment 2 examines the effect of adding cascade references (MFEncoder) to the Baseline, emphasizing the role of tile cascade generation in the map output. Results from these ablation experiments, displayed in Table III and Fig. 8, compare the generation outcomes of the Baseline method with those of the proposed method under 2X and 4X cascade references for map denoising. These experiments validate the effectiveness of each component in our approach and identify a more effective span for cascade generation.

1) *Effectiveness of Scale Information*: The scale feature adapter is designed to leverage scale information, aiding the generator in optimizing the output mapping at each level to represent content differences accurately. For example, in the map at level 16, the scale feature adapter effectively removes erroneous elements, such as an inappropriate yellow background and nonexistent roads. As shown in Table III, the

TABLE III
ABLATION RESULTS FOR CASCADE REFERENCE (MFENCODER) AND SCALE INFORMATION (CLIPENCODER) ON THE CSCMG DATASET.

| +MFEncoder | +CLIPEncoder | PSNR↑ | SSIM↑ | FID↓ |
|------------|--------------|---------------|--------------|---------------|
| × | × | 19.962 | 0.873 | 52.543 |
| × | ✓ | 20.898 | 0.882 | 44.217 |
| 2X | × | 23.096 | 0.934 | 45.512 |
| 2X | ✓ | 31.069 | 0.941 | 50.052 |
| 4X | × | 24.886 | 0.915 | 44.329 |
| 4X | ✓ | 31.584 | 0.935 | 34.369 |

addition of the scale feature adapter results in improvements across all metrics compared to the Baseline, particularly an increase of 8.3 in the FID score, underscoring the significant impact of scale information guidance on accurately representing map features. The CLIP-based scale information encoder translates the textual scale data of the generated map into image features, integrating these with ground features extracted from remote sensing images and embedding them into the pre-trained generator. This enables the model to discern comprehensive differences among maps of varying scales, leading to improved generation outcomes at each level that align more closely with the characteristics specific to those levels.

Fig. 8 illustrates the visualization results from the ablation experiment. Specifically, Fig. 8(c) shows the baseline results of map denoising based on remote sensing images, while Fig. 8(d) presents the outcomes after incorporating scale information. Maps generated with scale information exhibit superior visual quality compared to those produced without it. Notably, at level 16, the absence of scale constraints leads to erroneous geographic elements, such as the yellow background and roads. Incorporating scale information rectifies these inaccuracies, creating a more precise generated map.

2) *Effectiveness of Cascade Reference*: Adding cascade references to the multi-branch cartographic feature encoder



Fig. 9. Continuous Range Tile Map Generation: C2GM demonstrates powerful capabilities on generating wide-ranging, multi-scale, unbounded continuous, and virtually limitless tile maps.

(MFEncoder) aims to fuse low-level map information, further ensuring the consistency of the main content. As indicated in Table III, FID scores for generated maps with 2X and 4X cascade references are 45.512 and 44.329, respectively, while PSNR scores are 23.096 and 24.886. Compared to the scenario without cascade references, these FID scores reflect increases of 7.031 and 8.241, and PSNR scores show improvements of 3.134 and 4.924, respectively. Such results demonstrate that cascade generation significantly enhances the quality of the generated maps. Furthermore, an improved SSIM index indicates enhanced structural similarity of the generated maps, leading to more accurate outputs.

From Figures 8 (e) and (g), it is evident that considering multi-level information mitigates misjudgments of geographic elements that arise when only current-level data is analyzed. Visual discontinuities of geographic elements in the original map have been corrected, bringing the generated map closer to the actual representation. Results across different levels illustrate that employing a multi-branch cartographic feature encoder with cascade references allows for integrating single-level generated maps with information from other levels. This integration enables the cartographic model to better recognize objects' comprehensive features across various scales, thus acquiring more extensive cartographic expertise.

Moreover, Figures 8 (f) and (h) demonstrate that comparing the 2X and 4X cascade generation results from the ablation tests reveals superior outcomes for the 4X cascade generation in terms of FID, PSNR, and SSIM metrics. A broader cascade generation span facilitates the model's ability to learn comprehensive map features more effectively, resulting in more accurate maps. The performance of the 2X cascade generation may be limited by its narrower span, which could restrict the diversity of comprehensive map features the generation model can learn. Additionally, relatively similar cascade references may interfere with the terrain features extracted from the images, thereby diminishing the quality enhancement effect of the map cascade generation.

D. Comparison of the Map Tile Continuous Features of Cascade Generated

Notably, the large-scale tile map generation results achieved through the cascading generation method yield high-quality map images. When spliced together, several high-quality generated map tiles form a continuous tile map (Fig. 9). Although we employed a tile-by-tile generation approach, it is evident that the proposed method produces continuous surface features and maintains stylistic similarities between tiles. Our findings demonstrate that the cascading generation strategy reduces the visual discontinuity typically associated with tile splicing, making large-scale and multi-scale map generation easier. Furthermore, as illustrated in Fig. 7(k), the different scale maps generated for the same area exhibit varying degrees of comprehensiveness; for instance, the 18-level generated maps preserve more intricate details compared to the 16-level maps, much like authentic maps.

E. Comparison of the Cartographic Generalization Representation of Multi-Scale Generated

The experimental outcomes of multi-scale map generation reveal that utilizing low-level cascade reference map tiles for model training enhances the model's generalization capability at the scale level. Consequently, the proposed model can leverage the generated low-level map tiles as input to produce tile maps with higher resolutions and richer details. Fig. 8(h) illustrates the multi-scale cascade generation results of C2GM on the CSCMG dataset. In the initial phase, the model is conditioned on the existing map tiles of level 14, ultimately generating tile maps with map levels ranging from 15 to 18 based on remote sensing images and cascade references. This distinctive approach enables the creation of high-quality, multi-scale, large-scale tile maps encompassing diverse geographical features and ecosystems. As a generative model, C2GM unveils new avenues for constructing generative world models within geographic contexts by simulating the cartographic synthesis process employed by cartographers during the multi-scale mapping endeavor.

V. CONCLUSION

This paper presents C2GM, a groundbreaking generative foundation model tailored to large-span, multi-scale map cartography. By extending the capabilities of existing generative models, C2GM enables the creation of expansive, multi-scale tile maps across diverse geographical scenarios. The proposed self-cascading map generation framework, C2GM, integrated with the novel Scale-Guided Generation Model (SGDM), empowers map generation systems to produce high-quality tile maps characterized by rich geographical diversity, seamless visual continuity, and multi-level scale representations. This approach effectively addresses critical challenges related to model capacity, scale control, and cascaded generation. In addition, we developed the CSCMG dataset to facilitate the training and evaluation of multi-scale map generation models, incorporating cascaded reference and scale information. Comprehensive experiments on the CSCMG dataset underscore C2GM's exceptional capability in generating large-span tile maps. The advancements highlighted in this paper open new avenues for future research into the development of cross-modal cartographic models derived from multi-source remote sensing imagery.

REFERENCES

- [1] I. Goodfellow, J. Pouget-Abadie, M. Mirza, B. Xu, D. Warde-Farley, S. Ozair, A. Courville, and Y. Bengio, "Generative Adversarial Nets," in *Advances in Neural Information Processing Systems 27*, Z. Ghahramani, M. Welling, C. Cortes, N. D. Lawrence, and K. Q. Weinberger, Eds. Curran Associates, Inc., 2014, pp. 2672–2680.
- [2] P. Isola, J.-Y. Zhu, T. Zhou, and A. A. Efros, "Image-to-Image Translation with Conditional Adversarial Networks," in *2017 IEEE Conference on Computer Vision and Pattern Recognition (CVPR)*. Honolulu, HI: IEEE, Jul. 2017, pp. 5967–5976.
- [3] T.-C. Wang, M.-Y. Liu, J.-Y. Zhu, A. Tao, J. Kautz, and B. Catanzaro, "High-Resolution Image Synthesis and Semantic Manipulation with Conditional GANs," *arXiv:1711.11585 [cs]*, Aug. 2018.
- [4] J.-Y. Zhu, T. Park, P. Isola, and A. A. Efros, "Unpaired Image-to-Image Translation using Cycle-Consistent Adversarial Networks," *arXiv:1703.10593 [cs]*, Nov. 2018.
- [5] S. Ganguli, P. Garzon, and N. Glaser, "GeoGAN: A Conditional GAN with Reconstruction and Style Loss to Generate Standard Layer of Maps from Satellite Images," Apr. 2019.
- [6] X. Chen, S. Chen, T. Xu, B. Yin, J. Peng, X. Mei, and H. Li, "SMAPGAN: Generative Adversarial Network-Based Semisupervised Styled Map Tile Generation Method," *IEEE Transactions on Geoscience and Remote Sensing*, vol. 59, no. 5, pp. 4388–4406, May 2021.
- [7] Y. Fu, S. Liang, D. Chen, and Z. Chen, "Translation of Aerial Image Into Digital Map via Discriminative Segmentation and Creative Generation," *IEEE Transactions on Geoscience and Remote Sensing*, pp. 1–15, 2021.
- [8] Y. Liu, W. Wang, F. Fang, L. Zhou, C. Sun, Y. Zheng, and Z. Chen, "CscGAN: Conditional Scale-Consistent Generation Network for Multi-Level Remote Sensing Image to Map Translation," *Remote Sensing*, vol. 13, no. 10, p. 1936, May 2021.
- [9] Y. Fu, Z. Fang, L. Chen, T. Song, and D. Lin, "Level-Aware Consistent Multilevel Map Translation From Satellite Imagery," *IEEE Transactions on Geoscience and Remote Sensing*, vol. 61, pp. 1–14, 2023.
- [10] J. Ho, A. Jain, and P. Abbeel, "Denoising Diffusion Probabilistic Models," Dec. 2020.
- [11] J. Song, C. Meng, and S. Ermon, "Denoising Diffusion Implicit Models," Oct. 2022.
- [12] P. Dhariwal and A. Nichol, "Diffusion Models Beat GANs on Image Synthesis," Jun. 2021.
- [13] T. Wang, T. Zhang, B. Zhang, H. Ouyang, D. Chen, Q. Chen, and F. Wen, "Pretraining is All You Need for Image-to-Image Translation," May 2022.
- [14] C. Saharia, W. Chan, H. Chang, C. Lee, J. Ho, T. Salimans, D. Fleet, and M. Norouzi, "Palette: Image-to-Image Diffusion Models," in *Special Interest Group on Computer Graphics and Interactive Techniques Conference Proceedings*. Vancouver BC Canada: ACM, Aug. 2022, pp. 1–10.
- [15] W. Wang, J. Bao, W. Zhou, D. Chen, D. Chen, L. Yuan, and H. Li, "Semantic Image Synthesis via Diffusion Models," Nov. 2022.
- [16] L. Zhong, R. Onishi, L. Wang, L. Ruan, and S. J. Tan, "A Scalable Blockchain-based High-Definition Map Update Management System," in *2021 IEEE International Smart Cities Conference (ISC2)*, Sep. 2021, pp. 1–4.
- [17] R. Wang, H. Jiang, and Y. Li, "UPerNet with ConvNeXt for Semantic Segmentation," in *2023 IEEE 3rd International Conference on Electronic Technology, Communication and Information (ICETCI)*, May 2023, pp. 764–769.
- [18] X. Ma, X. Zhang, M.-O. Pun, and M. Liu, "A Multilevel Multimodal Fusion Transformer for Remote Sensing Semantic Segmentation," *IEEE Transactions on Geoscience and Remote Sensing*, vol. 62, pp. 1–15, 2024.
- [19] J. Zhang, X. Yang, R. Jiang, W. Shao, and L. Zhang, "RSAM-Seg: A SAM-based Approach with Prior Knowledge Integration for Remote Sensing Image Semantic Segmentation," Feb. 2024.
- [20] A. Toker, M. Eisenberger, D. Cremers, and L. Leal-Taixé, "SatSynth: Augmenting image-mask pairs through diffusion models for aerial semantic segmentation," Mar. 2024.
- [21] Z. Zhao, H. Bai, J. Zhang, Y. Zhang, S. Xu, Z. Lin, R. Timofte, and L. Van Gool, "CDDFuse: Correlation-Driven Dual-Branch Feature Decomposition for Multi-Modality Image Fusion," in *Proceedings of the IEEE/CVF Conference on Computer Vision and Pattern Recognition*, 2023, pp. 5906–5916.
- [22] D. Peng, P. Hu, Q. Ke, and J. Liu, "Diffusion-based Image Translation with Label Guidance for Domain Adaptive Semantic Segmentation," in *Proceedings of the IEEE/CVF International Conference on Computer Vision*, 2023, pp. 808–820.
- [23] J. Lu, G. He, H. Dou, Q. Gao, L. Fang, and Y. Deng, "ScoreSeg: Leveraging Score-based Generative Model for Self-Supervised Semantic Segmentation of Remote Sensing," *IEEE Journal of Selected Topics in Applied Earth Observations and Remote Sensing*, pp. 1–16, 2023.
- [24] C. Ayala, R. Sesma, C. Aranda, and M. Galar, "Diffusion models for remote sensing imagery semantic segmentation," in *IGARSS 2023 - 2023 IEEE International Geoscience and Remote Sensing Symposium*, Jul. 2023, pp. 5654–5657.
- [25] Z. Chen, D. Li, W. Fan, H. Guan, C. Wang, and J. Li, "Self-Attention in Reconstruction Bias U-Net for Semantic Segmentation of Building Rooftops in Optical Remote Sensing Images," *Remote Sensing*, vol. 13, no. 13, p. 2524, Jun. 2021.
- [26] B. Cheng, I. Misra, A. G. Schwing, A. Kirillov, and R. Girdhar, "Masked-Attention Mask Transformer for Universal Image Segmentation," in *Proceedings of the IEEE/CVF Conference on Computer Vision and Pattern Recognition*, 2022, pp. 1290–1299.
- [27] T. Shen, Y. Zhang, L. Qi, J. Kuen, X. Xie, J. Wu, Z. Lin, and J. Jia, "High Quality Segmentation for Ultra High-Resolution Images," in *Proceedings of the IEEE/CVF Conference on Computer Vision and Pattern Recognition*, 2022, pp. 1310–1319.
- [28] J. Jiang, C. Lyu, S. Liu, Y. He, and X. Hao, "RWSNet: A semantic segmentation network based on SegNet combined with random walk for remote sensing," *International Journal of Remote Sensing*, vol. 41, no. 2, pp. 487–505, Jan. 2020.
- [29] J. Yao, B. Zhang, C. Li, D. Hong, and J. Chanussot, "Extended Vision Transformer (ExViT) for Land Use and Land Cover Classification: A Multimodal Deep Learning Framework," *IEEE Transactions on Geoscience and Remote Sensing*, vol. 61, pp. 1–15, 2023.
- [30] F. Wang, J. Ji, and Y. Wang, "DSViT: Dynamically Scalable Vision Transformer for Remote Sensing Image Segmentation and Classification," *IEEE Journal of Selected Topics in Applied Earth Observations and Remote Sensing*, vol. 16, pp. 5441–5452, 2023.
- [31] X. Chen, Z. Liu, H. Tang, L. Yi, H. Zhao, and S. Han, "SparseViT: Revisiting Activation Sparsity for Efficient High-Resolution Vision Transformer," Mar. 2023.
- [32] Y. Li, J. Luo, Y. Zhang, Y. Tan, J.-G. Yu, and S. Bai, "Learning to Holistically Detect Bridges From Large-Size VHR Remote Sensing Imagery," *IEEE Transactions on Pattern Analysis and Machine Intelligence*, pp. 1–18, 2024.
- [33] S. Zhao, H. Chen, X. Zhang, P. Xiao, L. Bai, and W. Ouyang, "RS-mamba for large remote sensing image dense prediction," Mar. 2024.
- [34] S. Guo, L. Liu, Z. Gan, Y. Wang, W. Zhang, C. Wang, G. Jiang, W. Zhang, R. Yi, L. Ma, and K. Xu, "ISDNet: Integrating Shallow and

- Deep Networks for Efficient Ultra-high Resolution Segmentation,” in *2022 IEEE/CVF Conference on Computer Vision and Pattern Recognition (CVPR)*. New Orleans, LA, USA: IEEE, Jun. 2022, pp. 4351–4360.
- [35] J. Xi, O. K. Ersoy, J. Fang, M. Cong, T. Wu, C. Zhao, and Z. Li, “Wide Sliding Window and Subsampling Network for Hyperspectral Image Classification,” *Remote Sensing*, vol. 13, no. 7, p. 1290, Mar. 2021.
- [36] P. Luc, C. Couprie, S. Chintala, and J. Verbeek, “Semantic Segmentation using Adversarial Networks,” Nov. 2016.
- [37] Z. Chen, C. Wang, J. Li, N. Xie, Y. Han, and J. Du, “Reconstruction Bias U-Net for Road Extraction From Optical Remote Sensing Images,” *IEEE Journal of Selected Topics in Applied Earth Observations and Remote Sensing*, vol. 14, pp. 2284–2294, 2021.
- [38] X. Yang, J. Yang, Y. Yan, Y. Zhang, T. Zhang, Z. Guo, X. Sun, and K. Fu, “SCRDet: Towards More Robust Detection for Small, Cluttered and Rotated Objects,” in *Proceedings of the IEEE/CVF International Conference on Computer Vision*, 2019, pp. 8232–8241.
- [39] J. Ding, N. Xue, Y. Long, G.-S. Xia, and Q. Lu, “Learning RoI Transformer for Oriented Object Detection in Aerial Images,” in *Proceedings of the IEEE/CVF Conference on Computer Vision and Pattern Recognition*, 2019, pp. 2849–2858.
- [40] S. Yin, H. Li, and L. Teng, “Airport Detection Based on Improved Faster RCNN in Large Scale Remote Sensing Images,” *Sensing and Imaging*, vol. 21, no. 1, p. 49, Dec. 2020.
- [41] P. Li and C. Che, “SeMo-YOLO: A Multiscale Object Detection Network in Satellite Remote Sensing Images,” in *2021 International Joint Conference on Neural Networks (IJCNN)*. Shenzhen, China: IEEE, Jul. 2021, pp. 1–8.
- [42] J. Han, J. Ding, N. Xue, and G.-S. Xia, “ReDet: A Rotation-Equivariant Detector for Aerial Object Detection,” in *Proceedings of the IEEE/CVF Conference on Computer Vision and Pattern Recognition*, 2021, pp. 2786–2795.
- [43] C. Xia, X. Wang, F. Lv, X. Hao, and Y. Shi, “ViT-CoMer: Vision Transformer with Convolutional Multi-scale Feature Interaction for Dense Predictions,” in *Proceedings of the IEEE/CVF Conference on Computer Vision and Pattern Recognition*, 2024, pp. 5493–5502.
- [44] D. Muhtar, Z. Li, F. Gu, X. Zhang, and P. Xiao, “LHRS-Bot: Empowering Remote Sensing with VGI-Enhanced Large Multimodal Language Model,” Feb. 2024.
- [45] W. Zhang, M. Cai, T. Zhang, Y. Zhuang, and X. Mao, “EarthGPT: A Universal Multimodal Large Language Model for Multisensor Image Comprehension in Remote Sensing Domain,” *IEEE Transactions on Geoscience and Remote Sensing*, vol. 62, pp. 1–20, 2024.
- [46] K. Kuckreja, M. S. Danish, M. Naseer, A. Das, S. Khan, and F. S. Khan, “GeoChat: Grounded Large Vision-Language Model for Remote Sensing,” in *Proceedings of the IEEE/CVF Conference on Computer Vision and Pattern Recognition*, 2024, pp. 27 831–27 840.
- [47] X. Guo, J. Lao, B. Dang, Y. Zhang, L. Yu, L. Ru, L. Zhong, Z. Huang, K. Wu, D. Hu, H. He, J. Wang, J. Chen, M. Yang, Y. Zhang, and Y. Li, “SkySense: A Multi-Modal Remote Sensing Foundation Model Towards Universal Interpretation for Earth Observation Imagery,” in *Proceedings of the IEEE/CVF Conference on Computer Vision and Pattern Recognition*. arXiv, 2024, pp. 27 672–27 683.
- [48] U. Mall, C. P. Phoo, M. K. Liu, C. Vondrick, B. Hariharan, and K. Bala, “Remote Sensing Vision-Language Foundation Models without Annotations via Ground Remote Alignment,” Dec. 2023.
- [49] Y. Zhang, Y. Yin, R. Zimmermann, G. Wang, J. Varadarajan, and S.-K. Ng, “An Enhanced GAN Model for Automatic Satellite-to-Map Image Conversion,” *IEEE Access*, vol. 8, pp. 176 704–176 716, 2020.
- [50] J. Li, Z. Chen, X. Zhao, and L. Shao, “MapGAN: An Intelligent Generation Model for Network Tile Maps,” *Sensors*, vol. 20, no. 11, p. 3119, May 2020.
- [51] O. Tasar, S. L. Happy, Y. Tarabalka, and P. Alliez, “ColorMapGAN: Unsupervised Domain Adaptation for Semantic Segmentation Using Color Mapping Generative Adversarial Networks,” *IEEE Transactions on Geoscience and Remote Sensing*, vol. 58, no. 10, pp. 7178–7193, Oct. 2020.
- [52] X. Chen, B. Yin, S. Chen, H. Li, and T. Xu, “Generating Multiscale Maps From Satellite Images via Series Generative Adversarial Networks,” *IEEE Geoscience and Remote Sensing Letters*, vol. 19, pp. 1–5, 2022.
- [53] Y. Choi, M. Choi, M. Kim, J.-W. Ha, S. Kim, and J. Choo, “StarGAN: Unified Generative Adversarial Networks for Multi-Domain Image-to-Image Translation,” in *Proceedings of the IEEE Conference on Computer Vision and Pattern Recognition*, 2018, pp. 8789–8797.
- [54] J. Sohl-Dickstein, E. Weiss, N. Maheswaranathan, and S. Ganguli, “Deep Unsupervised Learning using Nonequilibrium Thermodynamics,” in *Proceedings of the 32nd International Conference on Machine Learning*. PMLR, Jun. 2015, pp. 2256–2265.
- [55] A. Nichol and P. Dhariwal, “Improved Denoising Diffusion Probabilistic Models,” Feb. 2021.
- [56] J. Ho, C. Saharia, W. Chan, D. J. Fleet, M. Norouzi, and T. Salimans, “Cascaded Diffusion Models for High Fidelity Image Generation,” *Journal of Machine Learning Research*, vol. 23, no. 47, pp. 1–33, 2022.
- [57] C. Saharia, J. Ho, W. Chan, T. Salimans, D. J. Fleet, and M. Norouzi, “Image Super-Resolution Via Iterative Refinement,” *IEEE Transactions on Pattern Analysis and Machine Intelligence*, pp. 1–14, 2022.
- [58] L. Zhang, A. Rao, and M. Agrawala, “Adding Conditional Control to Text-to-Image Diffusion Models,” in *2023 IEEE/CVF International Conference on Computer Vision (ICCV)*. Paris, France: IEEE, Oct. 2023, pp. 3813–3824.
- [59] R. Rombach, A. Blattmann, D. Lorenz, P. Esser, and B. Ommer, “High-Resolution Image Synthesis With Latent Diffusion Models,” in *Proceedings of the IEEE/CVF Conference on Computer Vision and Pattern Recognition*. arXiv, 2022, pp. 10 684–10 695.
- [60] C. Saharia, W. Chan, S. Saxena, L. Li, J. Whang, E. L. Denton, K. Ghasemipour, R. Gontijo Lopes, B. Karagol Ayan, T. Salimans, J. Ho, D. J. Fleet, and M. Norouzi, “Photorealistic Text-to-Image Diffusion Models with Deep Language Understanding,” *Advances in Neural Information Processing Systems*, vol. 35, pp. 36 479–36 494, Dec. 2022.
- [61] X. Wu, D. Zhang, R. Gan, J. Lu, Z. Wu, R. Sun, J. Zhang, P. Zhang, and Y. Song, “Taiyi-diffusion-XL: Advancing bilingual text-to-image generation with large vision-language model support,” Jun. 2024.
- [62] O. Avrahami, D. Lischinski, and O. Fried, “Blended Diffusion for Text-Driven Editing of Natural Images,” in *Proceedings of the IEEE/CVF Conference on Computer Vision and Pattern Recognition*, 2022, pp. 18 208–18 218.
- [63] S. Nie, H. A. Guo, C. Lu, Y. Zhou, C. Zheng, and C. Li, “The Blessing of Randomness: SDE Beats ODE in General Diffusion-based Image Editing,” Nov. 2023.
- [64] Y. Shi, C. Xue, J. H. Liew, J. Pan, H. Yan, W. Zhang, V. Y. F. Tan, and S. Bai, “DragDiffusion: Harnessing Diffusion Models for Interactive Point-based Image Editing,” Jun. 2023.
- [65] A. Hertz, R. Mokady, J. Tenenbaum, K. Aberman, Y. Pritch, and D. Cohen-Or, “Prompt-to-Prompt Image Editing with Cross Attention Control,” Aug. 2022.
- [66] H. Li, Y. Yang, M. Chang, S. Chen, H. Feng, Z. Xu, Q. Li, and Y. Chen, “SRDiff: Single image super-resolution with diffusion probabilistic models,” *Neurocomputing*, vol. 479, pp. 47–59, Mar. 2022.
- [67] A. Radford, J. W. Kim, C. Hallacy, A. Ramesh, G. Goh, S. Agarwal, G. Sastry, A. Askell, P. Mishkin, J. Clark, G. Krueger, and I. Sutskever, “Learning Transferable Visual Models From Natural Language Supervision,” Feb. 2021.
- [68] M. Cherti, R. Beaumont, R. Wightman, M. Wortsman, G. Ilharco, C. Gordon, C. Schuhmann, L. Schmidt, and J. Jitsev, “Reproducible scaling laws for contrastive language-image learning,” in *2023 IEEE/CVF Conference on Computer Vision and Pattern Recognition (CVPR)*, Jun. 2023, pp. 2818–2829.
- [69] A. Vaswani, “Attention is all you need,” *Advances in Neural Information Processing Systems*, 2017.
- [70] Z. Wang, A. Bovik, H. Sheikh, and E. Simoncelli, “Image quality assessment: From error visibility to structural similarity,” *IEEE Transactions on Image Processing*, vol. 13, no. 4, pp. 600–612, Apr. 2004.
- [71] M. Heusel, H. Ramsauer, T. Unterthiner, B. Nessler, and S. Hochreiter, “GANs Trained by a Two Time-Scale Update Rule Converge to a Local Nash Equilibrium,” in *Advances in Neural Information Processing Systems*, vol. 30. Curran Associates, Inc., 2017.
- [72] T. Park, M.-Y. Liu, T.-C. Wang, and J.-Y. Zhu, “Semantic Image Synthesis With Spatially-Adaptive Normalization,” in *Proceedings of the IEEE/CVF Conference on Computer Vision and Pattern Recognition*. Proceedings of the IEEE/CVF Conference on Computer Vision and Pattern Recognition, 2019, pp. 2337–2346.
- [73] C. Ledig, L. Theis, F. Huszar, J. Caballero, A. Cunningham, A. Acosta, A. Aitken, A. Tejani, J. Totz, Z. Wang, and W. Shi, “Photo-Realistic Single Image Super-Resolution Using a Generative Adversarial Network,” in *Proceedings of the IEEE Conference on Computer Vision and Pattern Recognition*, 2017, pp. 4681–4690.
- [74] Y. Pei, Y. Huang, Q. Zou, Y. Lu, and S. Wang, “Does Haze Removal Help CNN-based Image Classification?” in *Proceedings of the European Conference on Computer Vision (ECCV)*, 2018, pp. 682–697.